# The Along Track Scanning Radiometer for ERS-1—Scan Geometry and Data Simulation

A. J. FRED PRATA, ROBERT P. CECHET, IAN J. BARTON, AND DAVID T. LLEWELLYN-JONES

*Abstract*—**The first European Remote-sensing Satellite (ERS-1), due to be launched in 1990, will carry the Along Track Scanning Radiometer (ATSR) which has been specifically designed to give accurate satellite measurements of sea surface temperature (SST). Details of the novel scanning technique used by ATSR are given, and data from the NOAA-9 AVHRR instrument are used to simulate raw ATSR imagery.**

## I. INTRODUCTION

THE first remote-sensing satellite to be launched by the European Space Agency (ESA) during 1990 will carry a suite of instruments designed to provide valuable data related to the earth's oceans. Included in the payload is an instrument that has been specifically designed to measure sea surface temperature (SST) with an absolute accuracy that will make the data suitable for climate monitoring (the international Tropical Oceans Global Atmosphere, TOGA, program specifies an accuracy goal of 0.3 K [1]) and research. This instrument, the Along Track Scanning Radiometer (ATSR), is to be supplied to the ESA by a consortium of countries, including the United Kingdom, France, and Australia.

The ATSR has a channel at 1.6 $\mu$m, and 3 infrared channels that cover the same wavelength bands as the Advanced Very High Resolution Radiometer (AVHRR-2) on the operational NOAA satellites (3.6–3.9, 10.3–11.3, and 11.5–12.5 $\mu$m). Both instruments have similar spatial resolution at the surface (1.1 km at nadir). The ATSR, however, incorporates several design features that are expected to provide a far more accurate SST measurement than is currently available from satellite instruments. These features include improved on-board calibration, active cooling of detectors, dual-angle viewing of the earth's surface, and 12-bit resolution of the raw data transmission. Further details of the ATSR design characteristics are given by Delderfield *et al.* [2].

The capability of simultaneously (within 2 min) viewing the earth's surface from two different locations in space is an exciting feature of the ATSR. A conically scanning objective mirror gives a cross-track scan passing through the nadir, as well as a second scan forward of the subsatellite point (see Fig. 1). On the earth's surface these two scans are both curved and are separated by about 900 km on the subsatellite track. A further complication to the scan geometry is introduced by the "yaw steering" of the ERS-1 satellite. Here the satellite roll axis is moved away from the direction of flight to account for the rotation of the earth beneath the sun-synchronous satellite. The geometry of the ATSR scan mechanism, including the colocation of pixels in the two scans and the effect of yaw steering, is given in this paper. As the ATSR infrared channels span the same wavelength bands as those on the AVHRR, it is possible, using the ATSR and AVHRR scan geometries, to simulate the ATSR data stream by using data from the AVHRR. In this initial work allowance is made for the curved ATSR scans, yaw steering, and the extra atmospheric absorption of the radiances measured in the forward scan. The earth is assumed to be spherical and the orbit of ERS-1 is assumed to be circular. Figures are included which show the curved nature of the ATSR data, the increased absorption in the forward scan, and an example of SST determination using a combination of the ATSR nadir and forward views. The results presented will initially be used to test the standard ATSR data processing system that is under development at the Rutherford-Appleton Laboratory in the United Kingdom. Future devel-

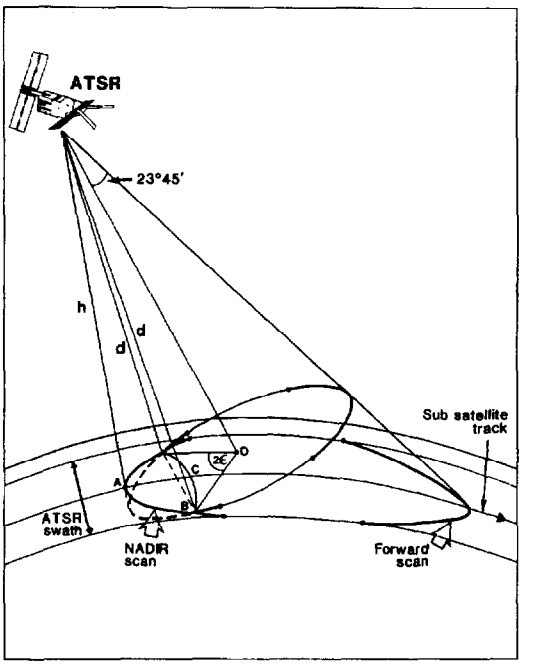


Fig. 1. Scan geometry for the ATSR instrument.

Manuscript received January 31, 1989; revised June 6, 1989.

A. J. Prata, R. P. Cechet, and I. J. Barton are with CSIRO, Division of Atmospheric Research, Station Street, Aspendale, Victoria 3195, Australia.

D. T. Llewellyn-Jones is with the Rutherford-Appleton Laboratory, Chilton, Didcot, Oxford, UK.

IEEE Log Number 8931110.

opments of the simulated data will include the many options available for the ATSR data stream, the variability in satellite altitude, the interleaving of the 1.6-$\mu$m channel data, and the on-board differencing of the 11- and 12-$\mu$m data. Later, cloud height and topographic effects may also be included. Meanwhile, the details of the ATSR geometry and the simulated images presented here give a first view of the data to be expected from the ATSR and may thus assist in various pre-launch activities.

## II. ATSR Scan Geometry

### A. ATSR Conical Scan

The ATSR rotating mirror causes the instrument beam to scan in a cone with a half-angle of $\beta$ (nominally 23.45°). Points on the earth's surface are scanned in a clockwise direction with the unit normal vector pointing downwards. The total scan is divided into 2000 pixels and the cone axis is tilted forward so that pixel number 501 is at the subsatellite point. The nadir scan is comprised of 555 pixels, while the forward scan is comprised of 371 pixels. Both scans cover a swath of approximately 500 km depending on the satellite altitude. The following equations can be used to determine the location of the ATSR pixels on the earth's surface relative to the subsatellite point. The angle of rotation ($\epsilon$) of the off-set mirror that traces out the conical scan is given by

$$\epsilon = 2\pi \left( \frac{p - 501}{2000} \right) \tag{1}$$

where $p$ is the pixel number ($p = 501$ is for the subsatellite point, and $p = 1501$ is for the central pixel in the forward scan). The zenith angle at the earth's surface $\chi$ is given by

$$\sin(\chi) = \sin(\alpha) \left[ \frac{R_e + h}{R_e} \right] \tag{2}$$

where $\alpha$ is the nadir angle at the satellite, $h$ is the satellite altitude, and $R_e$ is the earth's radius. Also, if $d$ is the distance between the satellite and the pixel location on the earth's surface, then

$$d \sin(\alpha) = R_e \sin(\chi - \alpha). \tag{3}$$

To calculate $\alpha$, we consider a right cross-section of the cone (a circle with center $O$) that intersects the earth's surface at the pixel location $B$ (see Fig. 1). Then

$$\sin\left(\frac{\alpha}{2}\right) = \sin(\beta) \sin\left(\frac{\epsilon}{2}\right). \tag{4}$$

If $B'$ is the complementary point on the opposite side of the subsatellite track on the earth's surface, then the straight line distance $BB'$ is given by

$$BB' = 2OB \sin(\epsilon) \tag{5}$$

and

$$d = \frac{OB}{\sin(\beta)}. \tag{6}$$

Thus, if the angle at the earth's center subtended by $BB'$ is $2a$, then

$$\sin(a) = \frac{BB'}{2R_e} \tag{7}$$

and combining (3), (5)–(7), we get

$$\sin(a) = \sin(\chi - \alpha) \sin(\epsilon) \frac{\sin(\beta)}{\sin(\alpha)} \tag{8}$$

where $a$ is also the angle at the earth's center that is subtended by the cross-track distance between the pixel and the subsatellite track. To calculate the along-track distance on the earth's surface, we need to consider the right spherical triangle on the earth's surface (shown in Fig. 2) that is determined by the pixel itself ($B$), the subsatellite point ($A$), and the point on the subsatellite track directly above the mid-point of $BB'$($C$). Napier's rules for right spherical triangles gives

$$\cos(b) \cos(a) = \cos(c) \tag{9}$$

where the distances on the earth's surface are specified in terms of the angle subtended at the earth's center. The angle $c$ is given by ($\chi - \alpha$) and gives the earth's surface distance between the pixel at $B$ and the subsatellite point, while $b$ gives the along-track distance. Typical earth's surface distances for the two ATSR scans are given in Table I, and the positions of some pixels and the hot and cold blackbodies are shown in Fig. 3.

### B. Yaw Steering

The principal mode of operation for the ERS-1 satellite is yaw steering, such that the satellite is slowly oscillated about its yaw axis to compensate exactly for the rotation of the earth beneath the satellite. The yaw angle $\Gamma$ is given by

$$\Gamma = \tan^{-1} \left[ \frac{(\sin^2(i) - \sin^2(\theta))^{1/2}}{\Omega_s/\Omega_e - \cos(i)} \right] \tag{10}$$

where $\theta$ is the latitude, $i$ is the inclination, $\Omega_e$ is the rotation rate of the earth, and $\Omega_s$ is the rotation rate of the satellite. This angle can easily be incorporated into the geometry above. The correction is of orbital frequency, a maximum at the equator, zero at latitudes $\pm(180 - i)$, and of opposite sign on the ascending and descending nodes. Yaw steering is used in order to compensate for the Doppler effect introduced by earth rotation in the wind measurements made by the scatterometer on-board the ERS-1 satellite. The effect of yaw steering on the ATSR forward scan swaths is shown in Fig. 4. The locus of points on the swath for a yaw-steered satellite is shown by the solid line. For reference, the dashed line shows the swath without yaw steering. The swaths are noticeably tilted with respect to the reference swaths and displaced westwards on both the ascending and descending nodes. A larger portion of the scan swaths covering approximately one orbit is shown for the nadir and forward views in Fig. 5. The effect of yaw steering is to shift the forward

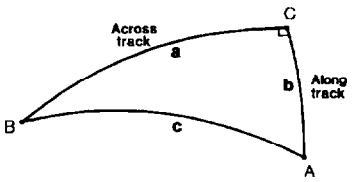


Fig. 2. The right spherical triangle bounded by the along-track distance, the across-track distance, and the distance from the pixel to the sub-satellite point.

TABLE I
LOCAL ZENITH ANGLE ($\chi$), CROSS-TRACK DISTANCE ($A$) AND ALONG-TRACK DISTANCE ($B$) FOR SELECTED PIXELS IN THE ATSR SCAN. THE EFFECT OF YAW-STEERING HAS NOT BEEN INCLUDED. VALUES ARE CALCULATED FOR A SATELLITE ALTITUDE OF 777 KM AND AN EARTH'S RADIUS OF 6371 KM. PIXELS 501 AND 1501 ARE ON THE SUBSATELLITE TRACK

| Pixel No. | $\chi$ (degrees) | a (km) | b (km) |
|---|---|---|---|
| *Nadir scan* | | | |
| 501 | 0 | 0 | 0 |
| 550 | 3.9 | 47.5 | 3.0 |
| 600 | 7.9 | 95.4 | 13.7 |
| 650 | 11.9 | 142.2 | 31.1 |
| 700 | 15.8 | 187.3 | 55.6 |
| 750 | 19.7 | 229.9 | 87.0 |
| 224/778 | 21.8 | 252.4 | 107.7 |
| *Forward scan* | | | |
| 1501 | 55.0 | 0 | 901.3 |
| 1550 | 54.8 | 74.8 | 892.8 |
| 1600 | 54.2 | 147.7 | 866.9 |
| 1650 | 53.2 | 213.9 | 825.5 |
| 1316/1686 | 52.3 | 256.0 | 787.6 |

scans into alignment with the nadir scans. The alignment is not exact, however, because the amount of yaw angle used compensates for earth rotation at the latitude of the sub-satellite point and not at the latitude of the forward scan. For pixels off the sub-satellite point the shift in across track distance due to this yaw angle does not exactly cancel the shift due to earth rotation.

### C. Satellite Altitude Changes

Changes in the altitude of the satellite cause changes in the panoramic distortion in the image. However, a more important effect is manifest in these data because of the dual-viewing capability of the ATSR. A change in the height of the satellite causes a movement in the relative positions of the nadir and forward views on the earth's surface. Derivation of accurate SST's relies crucially on being able to co-locate the dual-angle views. The effect of height changes on the positions of the pixels (as defined by the across- and along-track distances) has been estimated by assuming an ERS-1 reference orbit (shown in Fig. 6), calculating new along- and across-track distances and subtracting off the corresponding distances for a constant height orbit of 777 km. The results for the across- and along-track distances are shown in Fig. 7(a) and (b) for pixels on the edge and center of the swaths (pixels 224, 501, 778, 1316, 1501, and 1686). In these plots we have assumed no yaw steering. The actual distances on

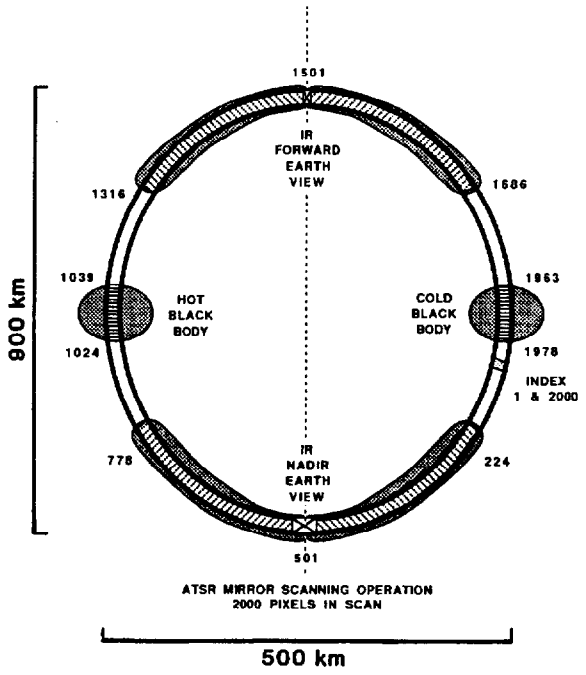


Fig. 3. ATSR pixel selection map showing locations of pixels and calibration sources (hot and cold black bodies) in a scan line.

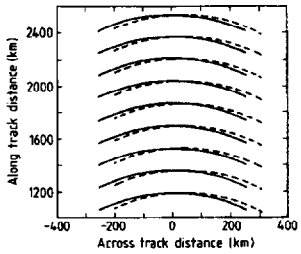


Fig. 4. Forward scan swaths for a portion of an ERS-1 satellite orbit, with yaw steering (solid line) and without yaw steering (dashed line).

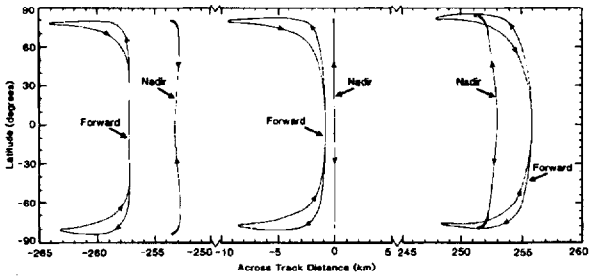


Fig. 5. Forward and nadir scan swaths with yaw steering for approximately one orbit. The arrows indicate the direction of flight of the ERS-1 satellite.

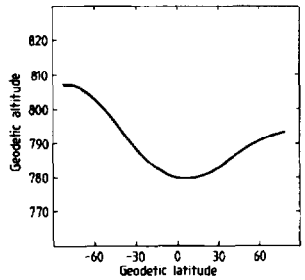


Fig. 6. ERS-1 reference orbit used to assess the effects of height changes on along- and across-track distances. Note that this orbit is only approximate and may not be the actual ERS-1 orbit used in flight.

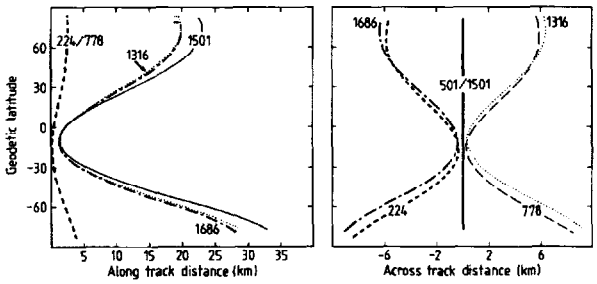


Fig. 7. (a) Difference in along-track distance for selected pixels on the earth's surface for a satellite with and without altitude changes. (b) Same as for (a), except that the difference is in the across-track distance.

the earth's surface from the subsatellite track for these pixels without yaw steering or altitude variations are shown in Table I. The effect of altitude changes is greatest on the along-track distance, which can be increased by up to 33 km. When yaw steering is included, the pixel locations are changed in both the along- and across-track directions and by amounts which are similar to or greater than those due to height changes (Fig. 8(a) and (b)). Note that although changes of up to 60 km or more occur, the total swath width for a given scan line is roughly the same with and without yaw steering and is only slightly increased due to altitude variations (cf. pixels 1316/1686 in Fig. 8(b)).

### *D. Stability of ERS-1*

The pointing accuracy required for the ATSR to meet its scientific goals (i.e., accurate SST) have been estimated to be 0.49° in pitch and roll and 0.60° in yaw. The ERS-1 platform is expected to be extremely stable and in addition the ESA plans to provide data at periodic intervals in order to characterize the attitude of the satellite. The anticipated overall pointing accuracies of ERS-1 are 0.14° in pitch and roll and 0.28° in yaw.

In order to achieve co-location of the forward and nadir views to within 1 pixel requires errors less than 0.08° in all three axes. Since these are unlikely to be met, pointing errors will be corrected by using identifiable points (e.g., landmarks) in the ATSR image. Also, the attitude data

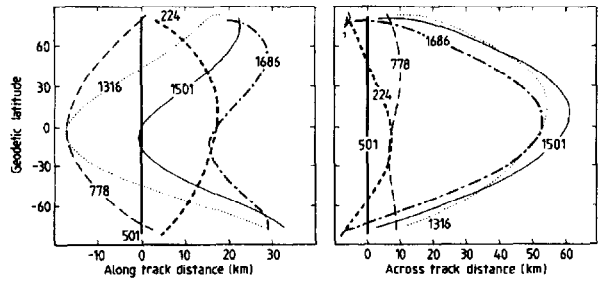


Fig. 8. (a) Difference in along-track distance for selected pixels on the earth's surface for a satellite with altitude changes and yaw steering, and for a satellite without altitude changes or yaw steering. (b) Same as for (a), except that it is for the across-track distance difference.

made available by ESA will be used to correct the forward and nadir data for stability changes. These data will be particularly useful when no landmarks are available; for example, over open ocean.

The nonstatic attitude error rates for roll, pitch, and yaw have been estimated to be 2.01 $10^{-3\circ}$ $s^{-1}$, 1.84 $10^{-3\circ}$ $s^{-1}$, and 1.61 $10^{-3\circ}$ $s^{-1}$, respectively. The corresponding time to accumulate an error of 1-pixel width is 37 s for roll, 40 s for pitch, and 63 s for yaw. Consequently, on a pixel-by-pixel basis it will not be possible to accurately combine information from the forward and nadir scans. However, for clear pixels over open ocean (i.e., away from land and steep temperature gradients), the required accuracy for overlap of the forward and nadir swaths is about 3 km. Although meeting this requirement would appear to be marginal, the figures quoted above are worst-case estimates, and it is expected that improvement will be made by including some post-processing attitude corrections.

## III. ATSR Data Simulation

A software package has been written to simulate ATSR data primarily to test processing schemes in preparation for the launch of ERS-1, but also to give potential users an opportunity to assess the usefulness of the data. In order to simulate ATSR data, we have used AVHRR thermal channel data from orbit 16290 of the NOAA-9 satellite received on February 10, 1988 at 0615 UT. A full width swath with the central region covering the southeastern corner of mainland Australia and the island of Tasmania was used, as the island has dimensions well-suited to exhibit the distortion produced by the conical scan of the ATSR.

Fig. 9 shows a false color image of the AVHRR scene used in the simulation. The enhancement of the image is produced by assigning red to AVHRR channel 2–channel 1, green to channel 2, and blue to channel 4. This particular enhancement shows the most vegetated areas of the image (e.g., forests) as orange to red, while leaving water surfaces colored blue, and clouds bluish white.

In the simulation method adopted we assume that the fictitious orbital trace of the ERS-1 satellite (carrying the

ATSR) coincides exactly with that of the NOAA-9 satellite (carrying the AVHRR). The inclinations of the orbits were assumed to be the same, but the corresponding heights were taken as 777 km for ERS-1 and 870 km for NOAA-9. The start location of the simulation corresponds to time $t = t_0$, where the AVHRR and ATSR are scanning at the same location relative to the earth's surface, and the ATSR is scanning line 1 and pixel 1 (see Fig. 3). The lines and pixels corresponding to a nadir scan angle of 0° (i.e., both instruments viewing vertically downwards) are (1,501) for the ATSR and ($l_0'$, 1024) for the AVHRR, where $l_0'$ is the earliest AVHRR line used in the simulation for the nadir scan. An added complication in the simulation arises because the forward scan receives data from 900-km "up-track" of the nadir scan. Consequently, at $t_0$, the moment the two subsatellite points are assumed to be coincident, the data from the forward scan has already been obtained.

As we are including yaw steering, the AVHRR data has been accurately navigated to allow the determination of the latitude of ERS-1 from AVHRR pixel and line numbers. Using the equations developed in Section II, the ATSR across-track distance ($R_x$) and along-track distance ($R_y$) are given by

$$R_x = R_e \sin^{-1}\left[\sin(A + \Gamma)\sin(A)\right] \tag{11}$$

$$R_y = R_e\Omega_s t + R_e \cos^{-1}\left[\frac{\cos(A)}{\cos\left(\frac{R_x}{R_e}\right)}\right]. \tag{12}$$

The angle $A$ is obtained from the spherical triangle shown in Fig. 2:

$$A = \sin^{-1}\left(\frac{\sin(a)}{\sin(c)}\right). \tag{13}$$

The ATSR line number $l$ is determined from

$$l = \frac{R_y}{R_e}\frac{\omega}{\Omega_s} \tag{14}$$

and the pixel number is given by (1).

Note that the yaw angle ($\Gamma$) has been included in these calculations. The distances are then used to determine the corresponding AVHRR pixel and line numbers.

### A. AVHRR Scan Geometry

The NOAA-9 polar-orbiting satellite flies in a sun-synchronous orbit, with an inclination near 98.8° at an altitude of 870 km above the earth's surface. The AVHRR instrument collects data by scanning perpendicularly to the direction of motion from an angle of 0° out to 55.4° on each side of the nadir, producing a swath over the surface of the earth of approximately 3000 km. The data acquisition rate is 360-lines per min, and 2048 samples (pixels) are obtained in each scan at equal increments in the scan angle. Each channel has an instantaneous field of view 1.3 mrad, yielding a spatial resolution of about 1 km at the subsatellite point, and at the edges of the swath 2.4 km along the satellite track by 6.8 km across the track. These have been calculated by using the equations given in the Appendix and are compared with the ATSR pixel sizes. Further details of the instrument may be found in Lauritson *et al.* [5].

Each of the ATSR nadir and forward scan coordinates (line and pixel) are related to the AVHRR scan coordinates through the across- and along-track distances on the earth's surface. The AVHRR orbital velocity, line scan rate, and angular scan increment are known; therefore the AVHRR line ($l'$) and pixel ($p'$) are

$$l' = l_0' + \frac{R_y}{R_e}\frac{\omega'}{\Omega_s'} \tag{15}$$

$$p' = 1024.5 + \frac{1}{\Delta\psi}\left(\tan^{-1}\left[\frac{\sin\left(\frac{R_x}{R_e}\right)}{\frac{R_e + h'}{R_e} - \cos\left(\frac{R_x}{R_e}\right)}\right]\right) \tag{16}$$

where $\Delta\psi$ is the AVHRR scan angle increment, $h'$ is the altitude of the NOAA-9 satellite, $\omega'$ is the line scan rate of the AVHRR, and $\Omega_s'$ is the orbital velocity of NOAA-9.

An ATSR line and pixel location does not normally correspond to a particular AVHRR line and pixel; therefore, the simulation software allows the user to select either the data from the nearest AVHRR line and pixel to the ATSR location, or a distance-weighted value over neighboring pixels.

### B. Simulated ATSR Image

The image displayed in Fig. 10 and on the front cover is produced by using a combination of data from AVHRR channels 1, 2, and 4 that has been processed with the ATSR simulation software. For an ATSR image, the scan mirror crosses the earth's surface in different directions for the two views, but in our image the two views are displayed in the correct sense so that intercomparison is possible. Also, the forward view has been displaced by approximately 900 km so that the two views span the same area. The simulated image shows clearly the curvature that will be present in both the ATSR views. The horizontal line near the top of the AVHRR image in Fig. 9 was produced by setting all the data in one scan line to be the maximum value. These pixels are transposed into the simulated images as curved lines. The curvature effect is also evident at the bottom corners of the forward view where no corresponding AVHRR data were available. The yaw-steering mode used by ERS-1 means that the satellite will look at an angle to the direction of the satellite motion, causing the center of the forward scan to be off the subsatellite track. This effect is seen in Fig. 10, where features[1] on the nadir scan are also seen in the forward

[1]Because of the opposite curvatures in each scan, some features to the north and south of the image are not duplicated.

scan, and vice versa. Another distortion present in all the images is due to the differences in the spacing between pixels and lines. The AVHRR image shows the island of Tasmania to be rather squat when compared to a map as a result of the difference between pixel and line spacing (0.8 and 1.09 km; see Appendix). In the nadir view the ATSR pixel and line spacing are almost equal, giving a more realistic image of the island.

## IV. Atmospheric Absorption

The accurate determination of SST from satellite data requires an estimate of the effect of atmospheric absorption and emission at the wavelengths sampled by the radiometer. This can be done by using differential absorption techniques. In the case of AVHRR data, the different absorption provided by 2 (or 3) infrared channels is used. For ATSR data, multiangle, as well as multichannel, techniques can be used, as the effect of absorption in the forward view at zenith angles near 55° should be approximately twice that for the nadir scan. In our ATSR data simulation the subsatellite tracks for both ATSR and AVHRR are taken to be coincident, and thus the data in the ATSR nadir scan already includes the atmospheric effect present in the AVHRR data. However, for the forward scan it is necessary to include some extra absorption to give realistic ATSR data. This is done in the following manner: Barton *et al.* [3] have used a band model of transmission through the atmosphere, with a data set of 74 radiosonde profiles to calculate theoretical satellite-measured radiances (or brightness temperatures), and have then derived linear algorithms for deriving SST from AVHRR and ATSR data. The algorithms are derived by using a regression procedure that minimizes the difference between the true and derived SST's. The band model of transmission was used to calculate the nadir scan values ($T_{3.7}$, $T_{11}$, and $T_{12}$) and the forward scan values ($T^f_{3.7}$, $T^f_{11}$, and $T^f_{12}$) for the subsatellite track and for selected distances off this track. The regression procedure was then used to calculate the coefficients in the following equations:

$$T^f_{3.7} = A_1 T_{3.7} + B_1 T_{11} + C_1 \tag{17}$$

$$T^f_{11} = A_2 T_{11} + B_2 T_{12} + C_2 \tag{18}$$

$$T^f_{12} = A_3 T_{11} + B_3 T_{12} + C_3. \tag{19}$$

Here the $f$ refers to the forward scan data, and $A$, $B$, and $C$ are the linear coefficients; i.e., the ATSR forward scan data are derived from the AVHRR nadir scan data. To account for the small effect of less absorption at the extremities of the forward scan (see the zenith angles in Table I), the coefficients include a term that is dependent on the cross-track range from the subsatellite track. Thus the coefficients are given by

$$(A_i, B_i, C_i) = (A'_i + A''_i d, B'_i + B''_i d, C'_i + C''_i d) \tag{20}$$

TABLE II
Coefficients for the Derivation of Simulated ATSR Forward-Scan Data from the AVHRR Values Using Equations (17)–(19). The Coefficients are Determined Using the Relation $A_i = A'_i + A''_i d$, etc., where $d$ is the Cross-Track Distance from the Subsatellite Track in km

| i | | $A', B', C'$ | $A'', B'', C''$ |
|---|---|---|---|
| 1 | $A_i$ | 0.80111E+00 | 0.21423E-03 |
| | $B_i$ | 0.18607E+00 | -0.20351E-03 |
| | $C_i$ | 0.24362E+01 | -0.19230E-02 |
| 2 | $A_i$ | -0.74385E-01 | 0.10438E-02 |
| | $B_i$ | 0.10764E+01 | -0.10473E-02 |
| | $C_i$ | -0.14146E+01 | 0.18331E-02 |
| 3 | $A_i$ | -0.10889E+01 | 0.11422E-02 |
| | $B_i$ | 0.20868E+01 | -0.11471E-02 |
| | $C_i$ | -0.49757E+00 | 0.23984E-02 |

where $d$ is the across-track distance (in kms) from the subsatellite point, and $i = 1$, 2, or 3. The linear coefficients are given in Table II. That this procedure for deriving the brightness temperatures for the forward-scan works can be tested by implementing an SST algorithm ($T_{11}$ and $T_{12}$) for the AVHRR data as well as an ATSR nadir- and forward-scan algorithm, and then comparing the SST's derived. This was done, and the rms difference between the AVHRR and ATSR SST's obtained from the algorithms was less than 0.1 K. The algorithms used are given by Barton *et al.* [3]. The AVHRR data taken from the ascending (daytime) pass over southeastern Australia includes an almost cloud-free image of the Island of Tasmania and the water between the Australian mainland and Tasmania (Bass Strait) and is suitable for determining the SST's. Fig. 11 shows the information displayed as the sea-surface temperature derived using the operational MCSST algorithm of McClain *et al.* [7].

Fig. 12 shows a simulated image of an ATSR 11-$\mu$m channel data. For the nadir view, the AVHRR Channel 4 data were used without any change to the pixel value. However, for the forward view extra atmospheric absorption was introduced as discussed in the previous section. In this image the land surfaces are colored black, the clouds white (or light blue), and the brightness temperature of the clear sea surface is colored from red for hot water to blue for cold water. The color wedge gives the brightness temperature values. The same scale has been used for both views and the effect of extra atmospheric absorption in the forward view is seen as a decrease in the brightness temperature of about 2 K. One of the features of the ATSR is its ability to correct for atmospheric absorption by using its dual-angle capability. Fig. 13 shows data from a section of the ATSR (and AVHRR) images which give an example of the SST derivation. The figure shows the 11-$\mu$m brightness temperatures and the SST derived from the data along the line drawn in Fig. 11. The SST was deduced using the appropriate algorithm given by Barton *et al.* [3]. This derivation is admittedly circu-

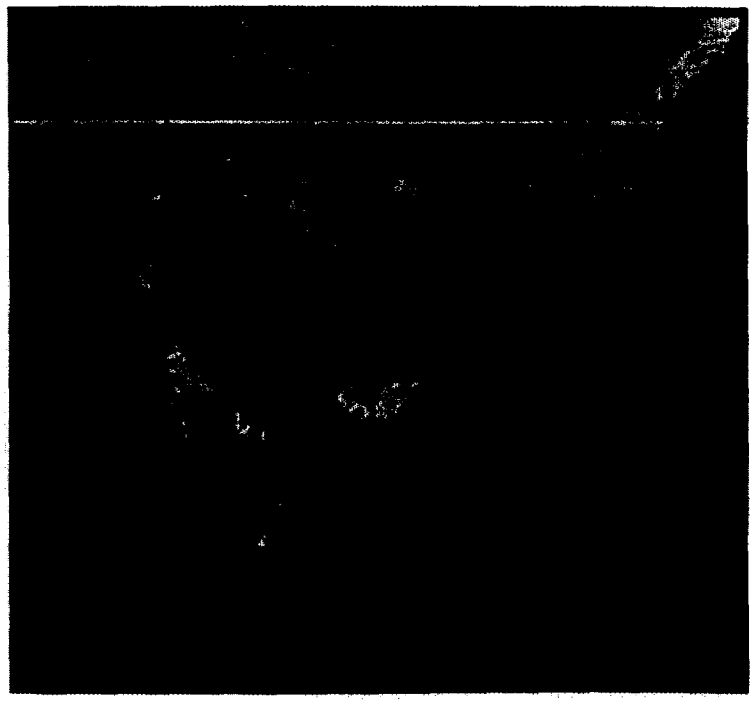

Fig. 9. The AVHRR image used for ATSR data simulation. The image has been enhanced by using channels 1 and 2 of the AVHRR to highlight land, sea, and cloud areas.

Fig. 10. The AVHRR image remapped in ATSR coordinates.

Fig. 11. Sea surface temperatures for the AVHRR image derived by using the algorithm of McClain *et al.* (reference [7]).

Fig. 12. Simulated ATSR images for the 10.8-μm channel.

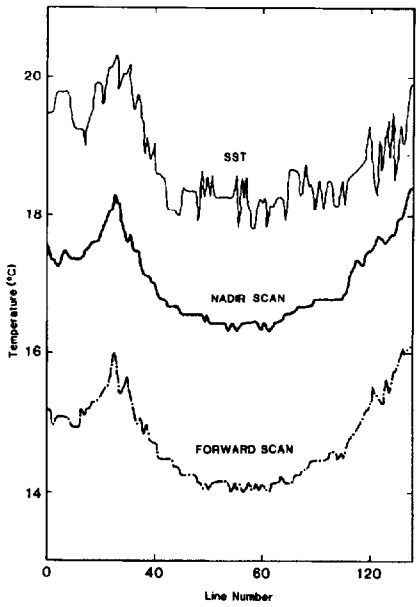


Fig. 13. Transect (white line on Fig. 11) showing the SST derived by using a typical theoretically derived SST algorithm.

lar, in that the forward data were derived using the same techniques, but the results do show how the ATSR system will operate. The increased noise which is evident in the SST is caused by the amplifying effect of the SST algorithm coefficients on the noise associated with channels 4 and 5 [6], [8], [4].

## V. Concluding Remarks

The ERS-1 satellite will provide data from a variety of instruments, principally for oceanographic purposes. The payload includes a scatterometer, an altimeter, and a synthetic aperture radar (SAR), as well as the ATSR and microwave radiometer. It is not appropriate to give details of these other instruments here, but it is important to note that many applications utilizing ATSR data will also use data from the other instruments. Although the main use of ATSR data will be for deriving global sea-surface temperature maps for climate models, experience from users of the AVHRR data indicates that ATSR data will also be used for a variety of land and atmospheric applications. Consequently, the list of applications of the data will be very similar to that of the AVHRR, and there will be additional applications which make use of the extra information contained in the forward view. Potential uses include land-surface temperature determination, lake area estimation to infer lake levels for climate studies, snow and ice monitoring, soil moisture and evapotranspiration estimates, and large-scale flood assessment. The use of the dual views for stereoscopic applications, such as cloud height determination [9], may also be possible.

One application that has been anticipated is the use of the 1.6-$\mu$m channel for studying ice- and snow-covered surfaces. Sea-ice extent and land-ice boundaries may be determined by using this channel. The channel will also be used to detect cloud-contaminated pixels in order to screen these from the SST processing.

In this paper, we have presented some details of the novel scanning technique employed by the ATSR and have shown what distortions will be present in the data due to geometrical effects and yaw steering. Because of the high precision of the on-board blackbodies, the active cooling of the detectors, 12-bit digitization, and dual-angle capability, the ATSR promises to achieve higher accuracy satellite-derived SST's than are currently available. The simulated ATSR data set described here is under continual development and should ultimately be useful for the testing of operational systems that are designed for ATSR data analysis.

## Appendix
## AVHRR and ATSR Pixel-Size Calculations

The AVHRR pixel semi-minor ($x$) and semi-major ($y$) axes dimensions of the eliptical pixels on the earth's surface are determined from the following equations:

$$y(\psi) = \frac{R_e}{2}\left\{\sin^{-1}\left[\frac{R_e + h'}{R_e}\sin\left(\psi + \frac{\phi}{2}\right)\right] - \sin^{-1}\left[\frac{R_e + h'}{R_e}\sin\left(\psi - \frac{\phi}{2}\right)\right] - \phi\right\}$$

$$x(\psi) = \frac{R_e}{2}\phi\frac{\sin(\chi - \psi)}{\sin(\psi)}$$

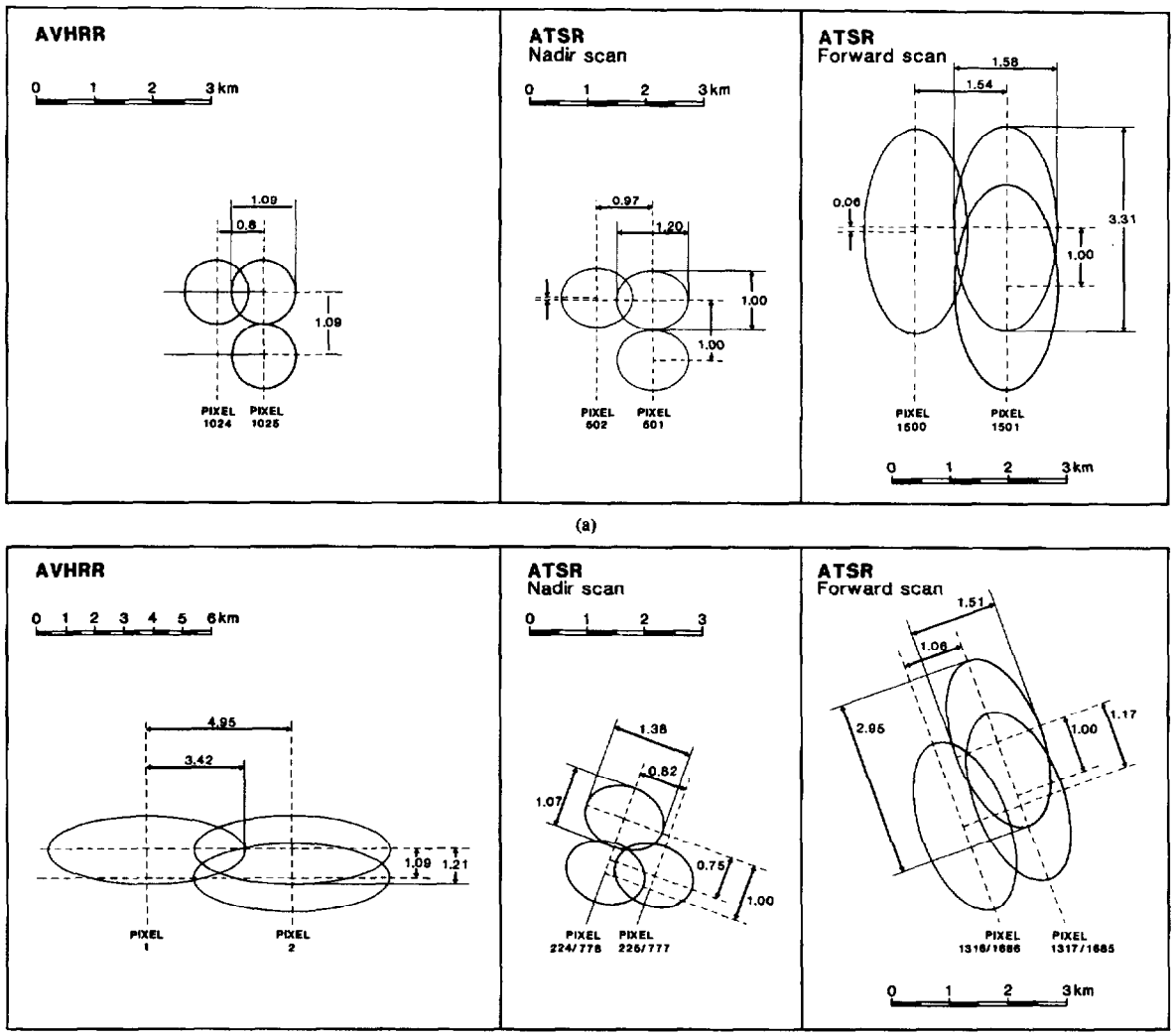


Fig. 14. (a) AVHRR pixel dimensions at nadir and at the edge of the swath. (b) ATSR pixel dimensions at the nadir and at the extreme scan angles.

where $\psi$ is the AVHRR nadir scan-angle, and $\phi$ is the angular field-of-view of the AVHRR in radians.

The ATSR instrument has a field stop which limits the field-of-view of the radiometer to 1.54 mrad in the across-track direction, and 1.29 mrad in the along-track direction. This information, combined with the appropriate ATSR scan-angle ($\alpha$, replacing $\psi$ in the equations above), can be used to determine the ATSR pixel semi-major and semi-minor axes dimensions. Fig. 14 shows the ATSR and AVHRR pixel sizes computed in this way at the center and the extremities of the scans. The figure has been drawn to scale to allow easy comparison between the different pixels. Also included in the figure is the along- and across-track distances between neighboring pixels on the same scan line.

## Acknowledgment

The mapping procedure was performed using CSIDA (CSIRO System for Interactive Data Analysis). The authors thank M. Dilley and C. Elsum for maintaining this facility.

## References

[1] World Climate Research Programme (WCRP), "Report on the TOGA workshop on sea surface temperature and net radiation," World Meteorological Org., Geneva, Switzerland, World Climate Programme Rep. WCP-92, 1984.

[2] J. Delderfield *et al.*, "The along-track scanning radiometer (ATSR) for ERS-1," in *Instrumentation for Optical Remote Sensing from Space*, J. S. Seeley, J. W. Lear, A. Monfils, S. L. Russak, Eds., *Proc. SPIE*, vol. 589, pp. 114–120, 1986.

[3] I. J. Barton *et al.*, "Theoretical algorithms for satellite-derived sea

surface temperatures," *J. Geophys. Res.*, vol. 94, no. D3, pp. 3365-3376, 1989.
[4] I. J. Barton, "Digitization effects in AVHRR and MCSST data," in *Remote Sensing Environ.*, to be published.
[5] L. Lauritson, G. J. Nelson, and F. W. Porto, "Data extraction and calibration of TIROS-N/NOAA radiometers," U.S. Dept. of Commerce, Washington, DC, NOAA Tech. Memo. NESS-107, 1979, 73 pp.
[6] P. E. La Violette and R. J. Holyer, "Noise and temperature gradients in multichannel sea surface temperature imagery of the ocean," *Remote Sensing Environ.*, vol. 25, pp. 231-241, 1988.
[7] E. P. McClain, W. G. Pichel, and C. C. Walton, "Comparative performance of AVHRR-based multichannel sea-surface temperatures," *J. Geophys. Res.*, vol. 90, pp. 11587-11601, 1985.
[8] A. F. Pearce, A. J. Prata, and C. R. Manning, "Comparison of NOAA/AVHRR-2 sea-surface temperatures with surface measurements in coastal waters," *Int. J. Remote Sensing*, vol. 10, no. 1, pp. 37-52, 1989.
[9] D. Lorenz, "On the feasibility of cloud stereoscopy and wind determination with the Along-Track Scanning Radiometer," *Int. J. Remote Sensing*, vol. 6, no. 8, pp. 1445-1461, 1985.

*

**A. J. Fred Prata** received the B.Sc.(Hons.) degree in physics in 1975, and the M.Sc. D.I.C. degree in atmospheric physics in 1978, both from Imperial College, London. In 1980 he obtained the D.Phil. degree from Oxford University for thesis work in stratospheric dynamics.

From 1978 until 1983, while at Oxford, his work was centered on theoretical and analytical studies of the stratosphere, utilizing data from the Nimbus 5, 6, and 7 satellites. In 1983 he emigrated to Australia and joined CSIRO, Aspendale, Vic., where he is a Senior Research Scientist in the remote sensing group of the Division of Atmospheric Research. He is involved in applications of satellite data to climate studies and is an ATSR science team member. His main research interests are in the use of satellite data for land-surface temperature determination and in radiative transfer studies in cloudy atmospheres at visible and infra-red wavelengths.

*

**Robert P. Cechet** received the B.Sc. degree in physics from the Chisholm Institute of Technology, Melbourne Australia, in 1979, and the Diploma of Meteorology from the Australia Bureau of Meteorology Training School in 1980.

He subsequently spent three years with the Bureau of Meteorology, working on public and aviation weather forecasting and acoustic sounding of the boundary layer, then an additional three years with the Australia Bureau of Mineral Resources, conducting geophysical field work in the Australian interior and Antarctica. In 1987 he joined the CSIRO Division of Atmospheric Research, Aspendale, Vic., to work on the ATSR project, in particular on the pre-launch ATSR data stream simulation program and the post-launch sensor calibration and temperature algorithm development program. More recently he has become interested in the use of satellite remotely sensed thermometry of the earth (land and sea surface) in the fields of agrometeorology and land-use management.

*

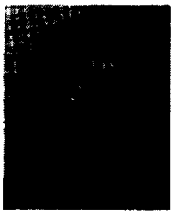

**Ian J. Barton** received the Ph.D. degree from Melbourne University in 1972.

Since then he has been working with the CSIRO Division of Atmospheric Research, Aspendale, Vic., where his early work was related to the use of passive microwave radiometry for the measurement of soil moisture. Since 1980 he has been concerned with the satellite derivation of surface temperatures using infrared radiometers. This has involved two lengthy sojourns in the UK, first at the University of Oxford in 1980, and then at the Rutherford-Appleton Laboratory in 1986. During the first of these visits the planning for the ATSR program was initiated, and the Australian involvement in the ATSR was consolidated during the second.

Dr. Barton is the Australian representative on the CEOS Working Group on Calibration and Validation, is a member of the ATSR Science Team, the Australian ERS-1 Science Committee, and the MODIS Science Team in NASA's Eos Program. In 1985 he was an invited delegate to the COSPAR workshop on Satellite-Derived Sea Surface Temperatures for Global Climate Applications.

*

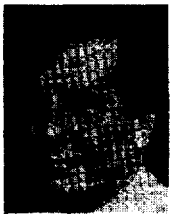

**David T. Llewellyn-Jones** obtained the Bachelor's degree in the UK, and received the master's and Ph.D. (1967) degrees from the Massachusetts Institute of Technology, Cambridge.

He then returned to work at the Appleton Laboratory, Slough, UK, and in 1981, following a merger between laboratories, he moved to the Rutherford-Appleton Laboratory, Chilton, where he is now Head of the Atmospheric Science Division in the RAL Space Science Department. His research activities have involved a number of technical and scientific aspects of infra-red and millimeter-wave physics, especially those concerned with atmospheric transmission, spectroscopy, remote sensing of the atmosphere from space, and related properties of the atmosphere. He is Principal Investigator for the Along-Track Scanning Radiometer (ATSR) instrument to be flown on the European Space Agency's ERS-1 satellite in 1990.